Scientia Iranica, Vol. 13, No. 2, pp 134–151

SCIENTIA
IRANICA

Experiments in Near-Field of Turbulent Jets into a Crossflow

K. Aavani[1], M. Taeibi-Rahni* and M.R. Soltani[2]

Low-speed wind tunnel experiments were conducted to examine the effects of jet exit behavior on the near-field characteristics of jets in crossflow. To better understand this problem, a row of six square jets were perpendicularly injected into the main turbulent flow. The jet-to-crossflow velocity ratios examined were 0.25, 0.5 and 1.0, while the jet spacing to jet diameter was 3.0. No significant temperature differences between the jet and the crossflow were introduced. The analysis of the vertical structure of the transverse jets, including focusing on the jet shear layer and the vorticity dynamics of the exiting jets, is complicated. The vorticity around the circumference of the jets was tracked to identify its relative contributions to the nascent streamwise vortices, which evolve eventually into kidney vortices downstream. The mean velocities and the six turbulent stresses were measured using a dual-sensor probe (X-array wire). Comparisons between the present work in the measurement sections with previous experimental data show reasonably good agreement. In this paper, the flow statistics are reported in the form of vector plots, contours and X-Y graphs, showing the velocity vectors, turbulence intensities and Reynolds stresses.

INTRODUCTION

Jets in crossflows have many practical engineering applications, including their use in primary combustion, fire extinguishers, industrial mixing, emergency venting, dispersion of pollutants, smokestacks, V/STOL transition flight aerodynamics, sewage, cooling water-outfalls and the film cooling of gas turbine blades. Such a flow field can be seen issuing from the exhaust stacks of most power plants and behind steam or diesel locomotives. In many of these applications, the resulting temperature downstream of the jet, the concentration of the hazardous material entering the crossflow from the jet or the trajectory and the physical path of the jet are important design parameters.

Jets in crossflows have also been used in industrial applications such as: film-cooling of turbines and combustors, fuel injection in burners, vectored thrust and thrust reversal for propulsive systems, pollutants emitted from chimneys and effluent discharged from pipes into rivers. For a non-circular exiting geometry of a jet, such as a square or rectangle, the leading-and trailing edge vortices are clearly distinguishable from the sidewall ones. Thus, the selection of square and rectangular holes enables us to separate the jet vortices that comprise the kidney vortices. The distinction between sidewall vorticity and that of leading and trailing edges, though blurred for a round hole, is distinguishable for a square or rectangular hole. The choice of non-circular holes makes it possible to reveal the unexpected double-decked structures of the streamwise vortices and link them to the vorticity generated along the walls of jet channels.

The lowermost vortex pair of double-decked structures, located beneath the jet, is what we call a "steady" vortex pair. This pair is always present and has the same sense of rotation as kidney vortices. The origin of these lower-deck vortices is the jet channel sidewall boundary layer; as the jet emanates from the hole, the crossflow forces the sidewall boundary layer to roll up into nascent kidney vortices. Here, the hole-width sets the lateral separation of these steady sidewall vortices. The upper vortices ride intermittently over the top of the "steady" lower pair. The sense of rotation of these upper-deck vortices depends on the hole geometry and can be the same as, or opposite to, the lower pair. The origin of the transverse to the crossflow direction is realigned with entrainment of the crossflow

1. *Aerospace Research Institute, Ministry of Science, Research and Technology, P.O. Box 14665-834, Tehran, I.R. Iran.*

*. *Corresponding Author, Department of Aerospace Engineering, Sharif University of Technology, P.O. Box 11365-8639, Tehran, I.R. Iran.*

2. *Department of Aerospace Engineering, Sharif University of Technology, P.O. Box 11365-8639, Tehran, I.R. Iran.*

momentum and, thus, induces a streamwise component of vorticity. Depending on the hole geometry, this induced streamwise vorticity can be opposite to the lower-deck vortex pair. The opposing pair, called the "anti-kidney pair", competes with the nascent kidney-vortices and affects the jet lift-off. The hole trailing-edge boundary layer can, likewise, be turned towards the streamwise direction. In this case, the turning is caused by the strong reverse flow just downstream of the jet.

Fric and Roshko [1], describe these primary vortices in such a flow. One is a ring vortex, which circumscribes the jet as it exits the jet channel. Another is a horse-shoe vortex in the near-field upstream of the jet exit (a result of the deceleration of the free stream fluid as it approaches the obstructing jet). The third is a wake vortex pair, which includes a Karman vortex street. This vortex pair is thought to be generated not at the jet to crossflow interface, but at the wall in the near jet region.

According to Anderopoulos [2], the near-field of the strong jets is controlled largely by complex inviscid dynamics, as opposed to that of a weak jet, which is turbulence dominated. Therefore, a weak jet (e.g., $R = 1.0$) may not exhibit all the characteristics described above. A configuration involving a row of jets introduces a new parameter, namely, the spacing-to-jet diameter ratio (S/D). For the extreme case of $S/D = 1.0$ (i.e., a 2-D slot), the jet penetration is strongest. As the spacing increases towards an intermediate value (somewhere between 3 to 5 diameters), the jet penetration decreases, partly due to the increasing entrainment of the free stream fluid [3]. As the spacing further increases, the free stream fluid begins to flow between the jets, thereby elevating the lee side pressure and causing the jets to penetrate deeper into the crossflow. The single jet marks the other extreme case of $S/D = \infty$, where the penetration is high. In turbine blade film cooling applications by discrete hole injection, typical design spacing corresponds to that of the weak jet penetration. This study is primarily concerned with multiple jets and low velocity ratios. Previous literature concerning single jets is still relevant and some examples of work involving such jets are cited below.

LITERATURE REVIEW

Many researchers have studied the flow of jets in a crossflow both computationally and experimentally. In 1946, Wieghardt [4] performed an experiment for two-dimensional turbulent film cooling. Also, in the late 1950's, Seban et al. [5], Chin et al. [6] and Papell and Trout [7] studied two-dimensional tangential film cooling. Since 1960, film cooled blades have been used, e.g., the M-88 engine of the Snecma Co. in France, which is still being used in Rafael planes. In that engine, they have been able to reduce the temperature of the air entering the turbine by about 300°C higher than its melting temperature.

In 1961, Hartnett et al. [8] used Wieghardt's geometric model and studied the effects of pressure gradient on film cooling. Later, Goldstein [9] reviewed and organized the works of previous investigators. Goldstein et al. [9] reported the effectiveness results for a circular hole. This was followed by a study by Goldstein et al. [10] that contrasted the single hole results with that of a row of holes. Pedersen et al. [11] presented the first open literature study of the effects of density ratio on film cooling. Their primary test surface geometry utilized holes angled 35° from the surface, directed in the downstream direction, with three-diameter hole spacing, but with holes half the diameter of the previous single row studies.

Ito et al. [12] reported the effects of curvature on film cooling effectiveness with density ratio varying from 0.75 to 2.0 and with a surface geometry of 35° holes spaced three diameters apart and with a mass flux ratio varying from 0.2 to 3.0. Katodani and Goldstein [13] examined the effects of boundary layer thickness, Reynolds number and free stream turbulence intensity on film cooling effectiveness and velocity and temperature distribution. They used a row of jets inclined at 35° to the mainstream direction issuing into the crossflow with velocity ratios between 1.5 and 2.0. The weak multiple jets issuing normally into a crossflow have been studied experimentally by Sugiyama and Usami [14], who reported pressure and mean velocities for a row of nine jets spaced at 3D and exiting at $R = 2.0$.

Foster and Lampard examined both effectiveness and concentration profile data and primarily studied the influence of injection angle (35°, 55° and 90°) and row spacing (1.25 to 3.0 diameter) on film cooling effectiveness for a range of mass flux ratios from 0.5 to 2.5 [15]. Khan et al. [16] reported jet concentration and mean velocities for $S/D = 2.0$ and $S/D = 4.0$ with $R = 2.3$ and compared their results to a coarse-grid numerical simulation. The data for the effects of a second row of holes with spacing 10 to 40 diameters downstream and with both 35° to 90° injection angles were presented by Afejuku et al. [17]. Issac and Jakubowski [18] used a hot-wire probe to measure mean velocities and five flow stresses in the region about tandem jets exiting at $R = 2.0$. Studies involving even lower velocity ratios, which better represent the application of the turbine blade film cooling, are less common. Forth et al. carried out a study of density ratio effects on film cooling from a single 30° row of holes with a three diameter hole spacing [19]. Teekaram et al. studied the effects of density ratio on film cooling heat transfer using two methods to achieve the density difference between the jets and the mainstream flow [15].

Pena and Arts [20] reported 2-component Laser-Doppler Velocimetry (LDV) measurements for velocity ratios as low as 0.5. They also varied the jet spacing from 3D to 5D and the jet density ratio from 1.0 to 2.0. Their primary interest was in the flow several diameters downstream of the injection hole. Two-component LDV velocity measurements were reported by Foucault et al. [21] on a row of 45° inclined jets exiting at $R = 0.6$ and 1.6. Distribution of temperature and temperature fluctuations were also reported in their paper. Some studies have examined the flow field in the region about a scaled model of a turbine blade (e.g., [22,23]). The geometry was simplified to a slot jet exiting a two-dimensional blade in both papers. Both experimental measurements and numerical simulations were performed by these authors. Normal jets in a crossflow have also been represented by numerical simulation.

Demuren [24] examined a single jet issuing into a crossflow at $R = 0.5$ and 2.0 with a finite volume multi-grid method and compared the results with those of Andreopoulos and Rodi. Kim and Benson [25] used a multiple time scale model to calculate the flow field of a row of jets for $R = 2.3$ and captured some interesting structures in the near jet region.

Ajersch et al. [26] have studied, both experimentally and computationally, the flow of a row of six rectangular jets injected at 90° to a crossflow. Their jet-to-crossflow velocity ratios (blowing ratios) examined were 0.5, 1.0 and 1.5 and their jet spacing-to-jet width ratio was 3.0. Also, their jet Reynolds number was 4700. No significant temperature differences between the jets and the crossflow were introduced. They used the LDV system operating in a three-component coincidence-mode, allowing for the measurements of three mean velocities and six flow stresses. Their numerical simulations of the flow were performed using a multi-grid, segmented, CFD code, using standard $k \quad \varepsilon$ turbulence modeling.

Taeibi-Rahni and Ebrahimi-Kebria [27] studied the film cooling of a flat plate at a Reynolds number of about 400 with circular holes using Direct Numerical Simulations (DNS). The equations in their study were solved using a finite difference explicit method of order 2 (in space and time) with a staggered grid. Their numerical method was projection and the black and red SOR (BRSOR) method was used for solving the pressure Poisson equation.

Asif Hoda and Acharya [28] studied the performance of several existing turbulence models for the prediction of a film coolant jet in a crossflow. Two equation models employing $k \quad \varepsilon$ and $k \quad \omega$ closure, broadly categorized as high-Reynolds number formulations, low-Reynolds number formulations, DNS-based formulations and non-linear formulations, have been used to simulate the flow. In all, seven different turbulence models have been tested. Predictions with different models have been compared with the experimental results of Ajersch et al. [26] and with each other to critically evaluate the model performance. The assessment of the models has been done, keeping in mind that all models have been formulated for wall-bounded flows and may not be well suited for the jet in crossflow situations. Close agreement with experimental results was obtained at the jet exit and for downstream of the jet injection region, but, all models typically overpredicted the magnitude of the velocities in the wake region behind the jet. Their study clearly underscores the deficiencies of the current models and demonstrates the need for improvement.

On the other hand, Keimasi and Taiebi-Rahni [29] performed calculations of a three-dimensional turbulent flow of square jets injected perpendicularly into a crossflow at a Reynolds number of 4700. Their jet to crossflow velocity ratios were 0.5, 1.0 and 1.5. They solved the Reynolds-averaged Navier-Stokes equations in its general form using the SIMPLE finite volume method over a non-uniform structured grid. For turbulence modeling, the standard $k \quad \varepsilon$ model with wall functions and the zonal $(k \quad \varepsilon)/(k \quad \omega)$ turbulence model (shear stress transport model) were used. Also, using Large Eddy Simulations (LES) and the Smagorinsky Subgrid Scale (SGS) model, Ramezani-Zadeh and Taiebi-Rahni solved the same problem [30]. The results of these two works agreed well compared with existing benchmark data.

EXPERIMENTAL FACILITY AND SETUP

The wind tunnel used to generate the crossflow was an open-loop blow-down tunnel with a maximum air speed of 35 m/s. The test section was 1200 mm long and had a 450 mm × 450 mm cross-section dimension. To ensure that a fully turbulent boundary layer was present in the test section, a 2.4 mm rod was affixed to the tunnel wall at the test section entry. The details of the test section geometry are shown in Figure 1a. A row of six square jets was arranged on the tunnel wall, 450 mm downstream of the boundary layer trip. The row was oriented perpendicular to the direction of the crossflow and the jets were issued into the crossflow at an angle of 90° to the plane of the tunnel wall. Each jet measured 12.7 mm × 12.7 mm in cross-section and had an entry length of 6 diameters. The spacing between the jet centerline was 3 diameters. The entries to the jet channels were sharp-edged, as opposed to nozzle-shaped. The airflow for the jets was supplied by a 4.0 bar (static) compressed air line and was regulated by an air filter regulator. There were also a mist separator and a flow rate indicator in the line. A plenum (or

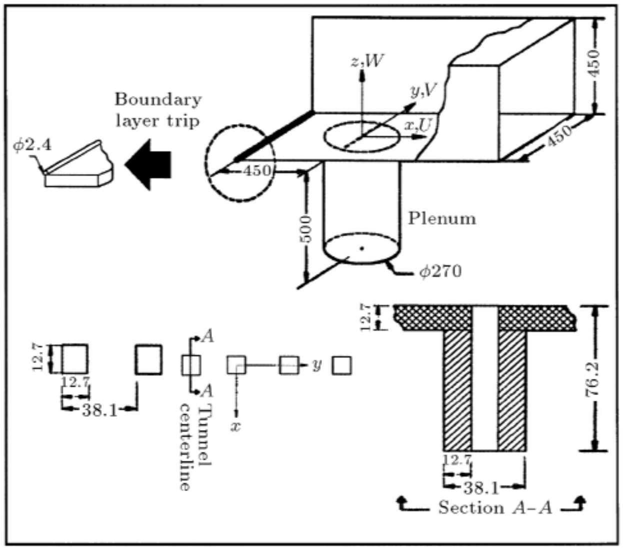

Figure 1a. The test section geometry and the details of the jet exit (all dimensions are in mm).

settling chamber) with a 270 mm diameter and 500 mm height was positioned on the channel wall between the air line and the jet channels. The coordinate system used in this experiment is shown in Figure 1a. The flow field characteristics of the jets in a crossflow are strongly dependent on the momentum ratio, which is defined as:

$$J = \frac{\rho_{\mathrm{jet}} V_{\mathrm{jet}}^2}{\rho_{\mathrm{cf}} V_{\mathrm{cf}}^2}. \tag{1}$$

In this low-speed isothermal experiment, since the same fluid is used in the crossflow and in the jet, the densities in Equation 1 cancel and, thus, the relevant parameter becomes the velocity ratio, R. Three cases of R were examined here, namely, 0.25, 0.5 and 1.0 (i.e., $J = 0.0625$, 0.25 and 1.0, respectively). Throughout the experiment, the bulk jet velocity was maintained at 5.5 m/s. Therefore, the crossflow velocities used were 5.5, 11.0 and 22.0 m/s. Based on the jet diameter of 12.7 mm and the viscosity of the air at standard pressure and temperature, the jet Reynolds number was fixed to be constant at approximately 4700.

MEASURING TECHNIQUES

The flow statistics for this experiment were obtained by Hot-Wire Anemometry (HWA). A dual-sensor probe (X-array wire) was used to measure the flow field characteristics. Note, an X-probe can also be used for multi-position measurements, provided that it can be rotated around its stem. If the probe-stem is aligned with a mean flow direction and the turbulence intensity is low, then, simultaneous measurement of two velocity components can be obtained at any roll-angle position. The velocity components and the Reynolds stresses evaluated were transformed into the corresponding space-fixed components using transformation equations. Note, if the procedure were repeated three more times (after rolling the probe about its axis to positions 45°, 90° and 135°, with respect to the starting position) the results could be combined to obtain all three mean velocity components, six Reynolds stresses and the ten triple products [31-33]. A traverse mechanism with three degrees of freedom was applied in order to place the hot-wire probe at all the required measurement points and to fulfill all the angle positions needed for data acquisition. The procedure for the flow field measurements, data acquisition setup and probe calibration method by application of an X-hot wire are described, in detail, below.

Three-Dimensional Flow Field Measurements

The most common procedure for data analysis with X-probes is the sum and difference method. This procedure deals with two simultaneous signals obtained from an X-probe. It ignores the "cooling-effect" of the third component, which is perpendicular to the hot wire plane (when it exists). Therefore, the method is applicable only if the magnitude of the third component (W) is small in comparison to the other two components (U and V). In this study, the cross-tunnel velocity is very small in comparison with the streamwise and the normal velocity components. From the instantaneous velocity records, the mean velocities (as well as the Reynolds stresses) were determined. The mean velocities (u, v and w) were evaluated by time averaging. The assumptions usually made in the implementation of the crossed hot-wire technique include: (i) The variation of the instantaneous velocity between the two wires is negligible; (ii) The variation of the instantaneous velocity along the active region of a given wire is negligible; (iii) The mean velocity vector is roughly aligned with the axis of the probe; and (iv) The velocity fluctuations are small fractions of the mean velocity. Note, the effects of the variation of the velocity along a given wire are of a higher order than the effects of the wire-to-wire variations. Thus, these effects do not need to be considered in the present work.

Calibration and Data Acquisition Setup

In order to calibrate the X-hot wire probe, a flow master sensor was used to accurately measure the wind tunnel mainstream velocity at different values in our velocity range. The probe is placed normal to the mainstream of the wind tunnel. The real time data was recorded by a computer program from two channels of an Analogue to Digital Converter Board (A/D).

Our X-hot wire probe in this work consisted of two single slanted hot wires (Dantec 55P51). The plane of the wires identifies the measuring plane. Thus, the calibration procedure for an X-probe is similar to that for a single yawed hot wire probe. In this work, the calibration equation for each wire is a full 4th order polynomial in voltage to achieve high accuracy and to minimize any calibration errors. The normalized standard deviation for this polynomial-fit is much smaller than the power-law method [34]. The data acquisition setup and the schematic of the cross-section of the wind tunnel test section of this study are shown in Figure 1b. Also, the schematic pictures in the laboratory are shown in Figures 2a and 2b.

UNCERTAINTY ESTIMATES

Uncertainty estimates are based on 95 percent confidence levels and determined using the methods de-

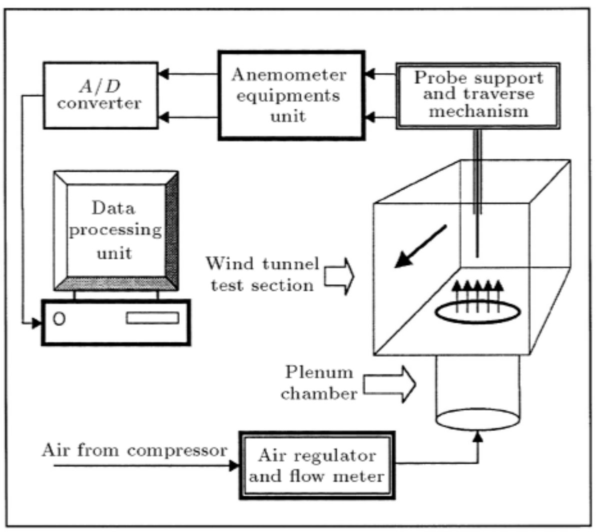

Figure 1b. The data acquisition setup and arrangement of hot-wire probe with respect to the test section.

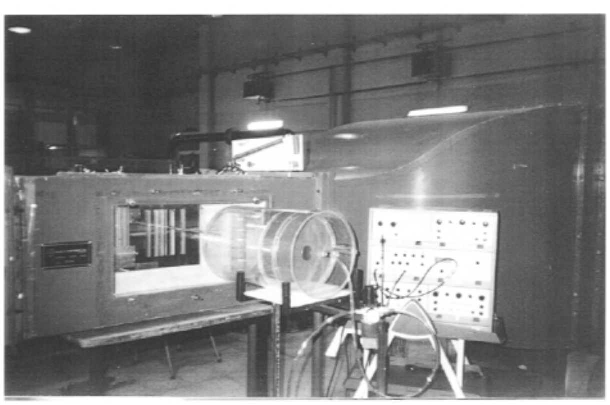

Figure 2a. Picture of plenum chamber and six square jets injection setup to the mainstream of wind tunnel.

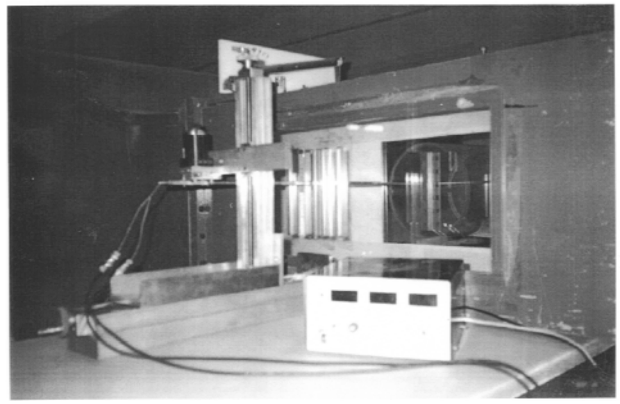

Figure 2b. Picture of the data acquisition setup and arrangement of hot-wire probe with respect to the test section.

scribed by Kline and McClintock [35] and by Moffat [36]. The data presented in this paper were typically averaged over 5,000 points or more, depending on the data rate. The bias uncertainty for the mean velocities is about 0.4 percent, whereas the precision uncertainties were 1 percent in the free stream and 3.4 percent near the wall. The precision uncertainty for the RMS velocity measurements was 1.4 percent in the free stream and 4.6 percent near the wall. The uncertainty of the turbulent shear stress was about 5.3 percent.

RESULTS AND DISCUSSIONS

The experimental data in some of the common setups and measurement sections were compared with the experimental results of Ajersch et al. [26], shown in Figure 3 for two velocity ratios (0.5 and 1.0). The results are divided into the ones related to the jet-exit conditions with no crossflow, the jet-exit conditions, the mean velocity field, the mean velocity profile, the Reynolds stress distributions, the turbulence intensities and the anisotropy. Due to symmetry of injection, the results are shown for one jet in the induced effects of side by side jets.

Jet-Exit Conditions with no Crossflow

The flow field in the jet's plane ($z/D = 0$) with no crossflow is shown in Figure 4. Figure 4a shows the streamwise velocity contours in this plane. As expected, the mean streamwise velocity is very small and the ratio (u/V_{jet}), due to the momentum of jet stream and the small fluctuations of velocity components in streamwise and cross-tunnel velocity, is negative in some regions. Figure 4b shows the normal velocity contours for six rectangular jets. In this figure, as expected, the normal velocity at the jet center is maximized. However, due to the wall friction, this velocity is much less near the surface. Also, Fig-

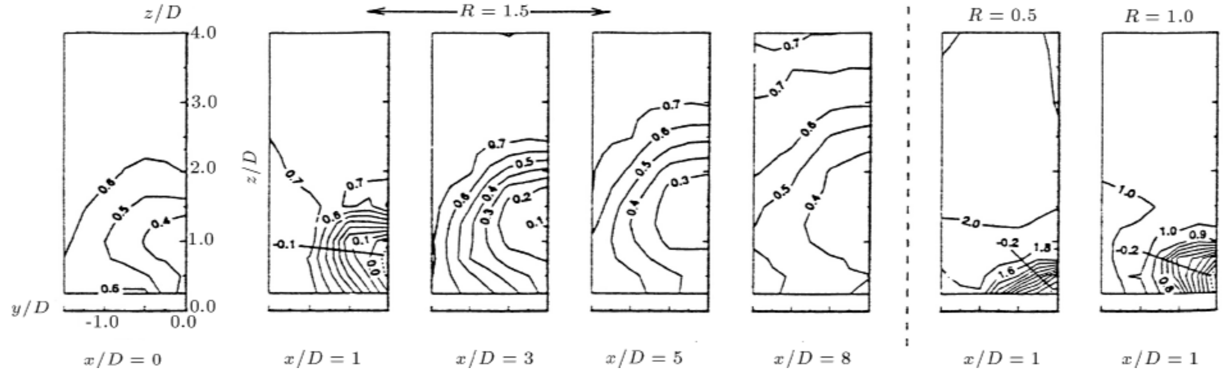

Figure 3a. The streamwise velocity (u/V_{jet}) in cross-tunnel planes for $R = 0.5$, 1.0 and 1.5 at different spanwise locations, $x/D = \{0, 1, 3, 5 \text{ and } 8\}$ [26].

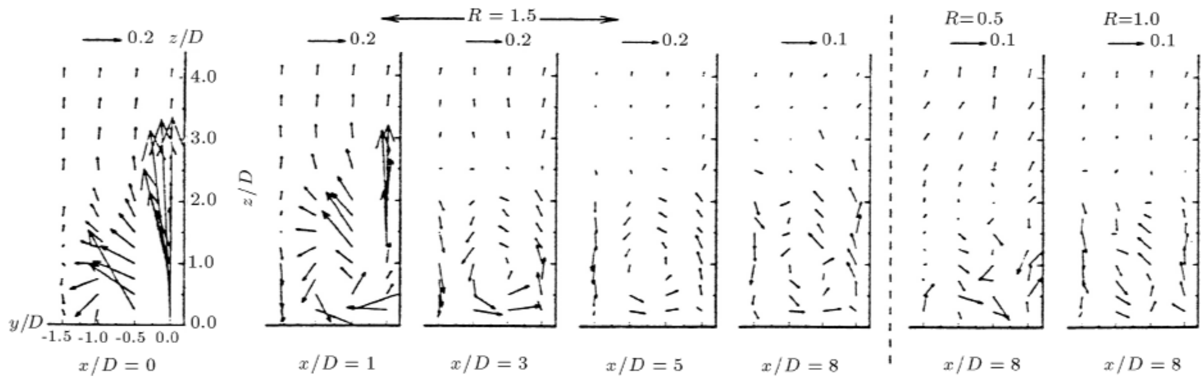

Figure 3b. The velocity normal to the main stream velocity (v/V_{jet}) in cross-tunnel plane for $R = 0.5$, 1.0 and 1.5 at different spanwise locations, $x/D = \{0, 1, 3, 5 \text{ and } 8\}$ [26].

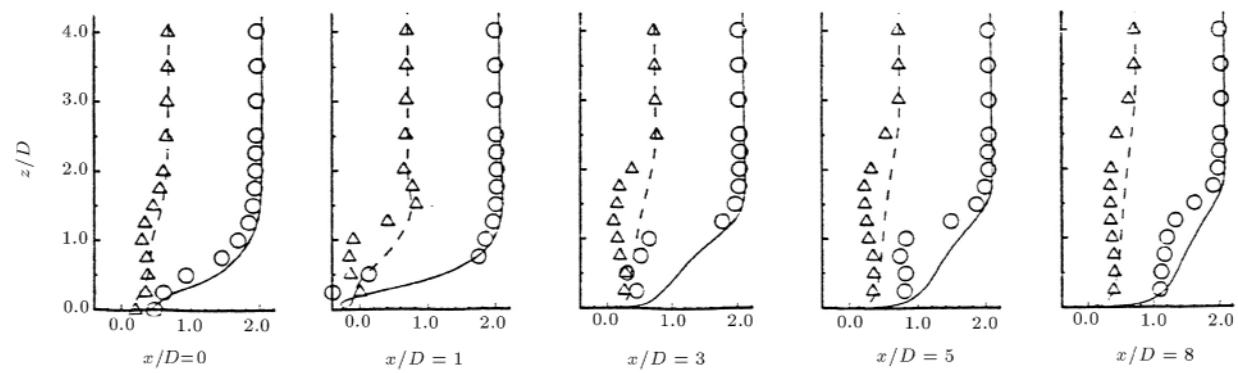

Figure 3c. The streamwise velocity profile (u/V_{jet}) for ($y/D = 0$). Measured for: $R = 1.5$ (△), $R = 0.5$ (○), Computed for: $R = 1.5$ ( ), $R = 0.5$ (———) at different spanwise locations, $x/D = \{0, 1, 3, 5 \text{ and } 8\}$ [26].

ure 4c shows the non-dimensional cross-tunnel velocity (v/V_{jet}) contours in the jet exit plane ($z/D = 0$). As expected, the lateral velocity was affected by the acoustics of jets discharging to the quiescent air and the local minimum was occurred in proximity of the holes due to the lateral interaction of the double-deck kidney vortices.

The turbulence kinetic energy ($\sqrt{k}/V_{\text{jet}}$) contours in the jet exit plane ($z/D = 0$) are shown in Figure 5. In this figure, due to the momentum of the jet stream, the weak interactions between longitudinal and lateral fluctuations of the velocity field (with respect to the coordinate system on the hole center plane) and the breakdown of large eddies at the entrance of the jet's channels (the diffusion due to the turbulent boundary layer of the jet stream), the turbulence kinetic energy at the core of the jets is minimum and increases to maximum intensity at the sidewalls of the holes. Note that the other jet's intensity parameters are also measured here.

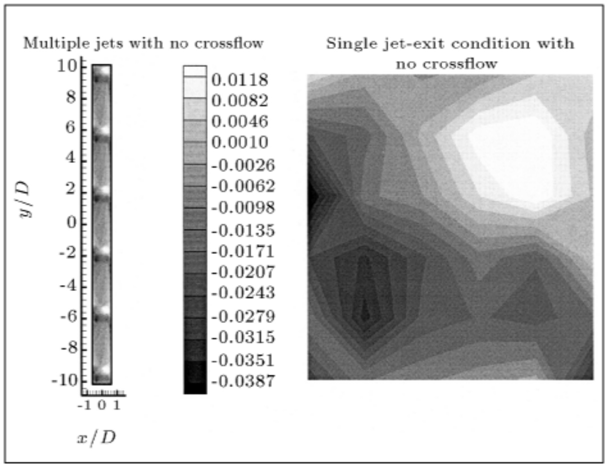

Figure 4a. The streamwise velocity (u/V_{jet}) for single jet and multiple jets with no crossflow.

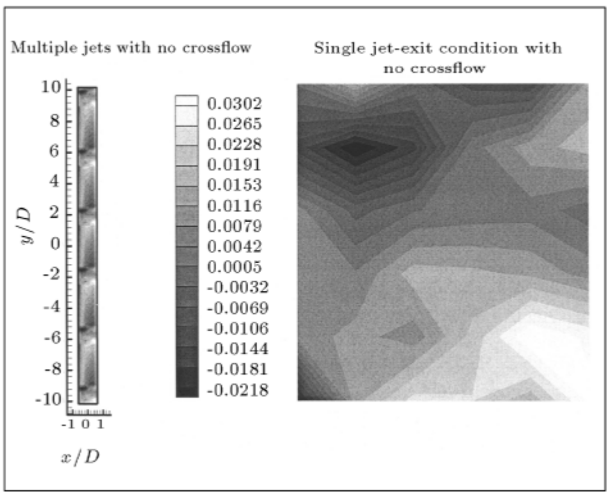

Figure 4b. The cross-tunnel velocity (v/V_{jet}) for single jet and multiple jets with no crossflow.

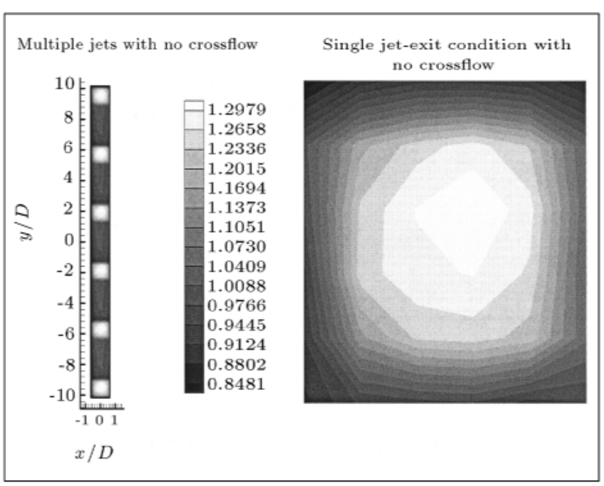

Figure 4c. The normal velocity (w/V_{jet}) for single jet and multiple jets with no crossflow.

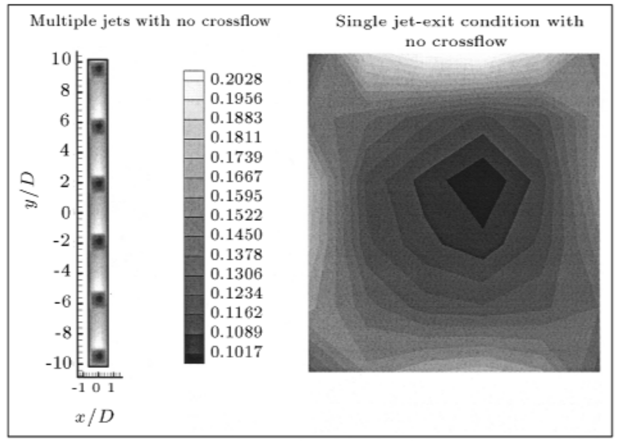

Figure 5. The turbulence kinetic energy ($\sqrt{k}/V_{\text{jet}}$) for single jet and multiple jets with no crossflow.

Jet-Exit Conditions

The measured data show that the jet and the crossflow interact strongly. Also, the flow field at the jet exit heavily depends on the jet to the crossflow velocity ratio. The non-dimensional vertical velocity contours at the jet exit for three different velocity ratios (0.25, 0.5 and 1.0) are shown in Figure 6. Figure 6a represents our experimental results, while Figure 6b shows Ajersch's experimental data [26]. Comparison of Figures 6a and 6b (at velocity ratios 0.5 and 1.0) demonstrates that the vertical velocities obtained by our measurements agree well with Ajersch's data [26]. For all velocity ratios, the variation of $(\widetilde{V}/V_{\text{jet}})$ on the upstream half is higher than that for the downstream one. However, the profile becomes more uniform for high velocity ratios [37].

The non-dimensional velocity vectors in the jet exit plane are shown in Figure 7. The authors' experimental results show close agreement with Ajersch's results. The streamwise deflection of the jet in all cases is shown very clearly in this figure and, as expected, it is the strongest for the case $R = 0.25$. Also, the transverse deflection exists and its value is increased by distance away from the jet centerline. These results show symmetry about the centerline ($y/D = 0$) in all three cases. Note that in the experimental setup used in this work, the quiescent fluid of the plenum chamber accelerates around the sharp edges of the inlet and then into the jet channel. This leads to the non-uniformity of the turbulence kinetic energy.

Mean Velocity Field

The most important feature of the jet in a crossflow is the interaction between the two crossing flows. In this study, as expected, when the jet-to-crossflow velocity ratio increases, the jet penetration is enhanced. For $R = 0.5$, the jet flow stays inside the boundary layer (in

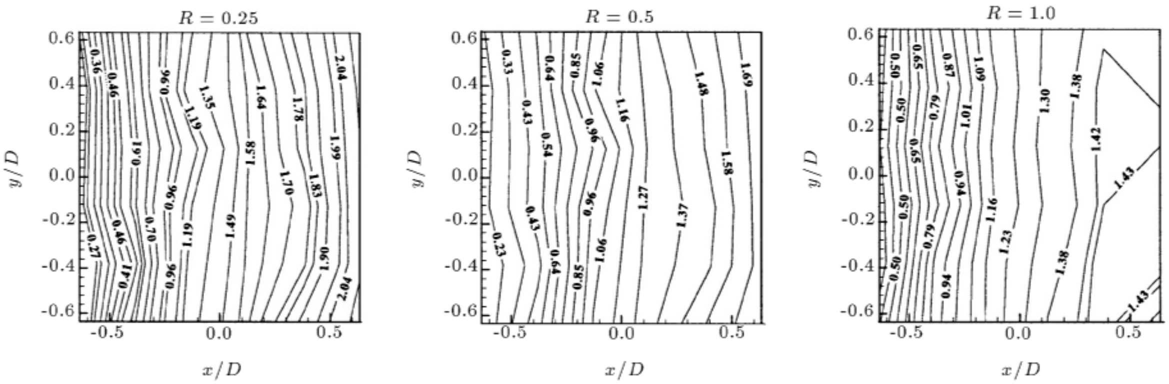

Figure 6a. The vertical velocity (w/V_{jet}) at the jet exit plane.

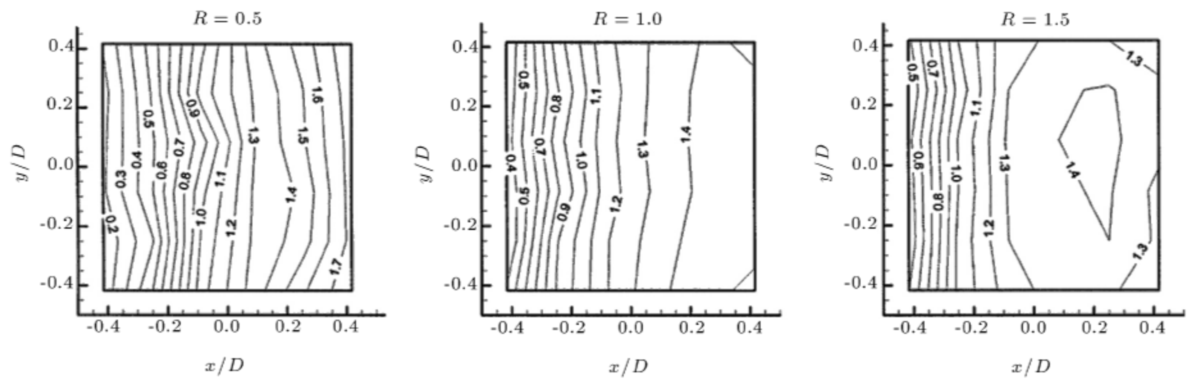

Figure 6b. The vertical velocity (w/V_{jet}) at the jet exit plane [26].

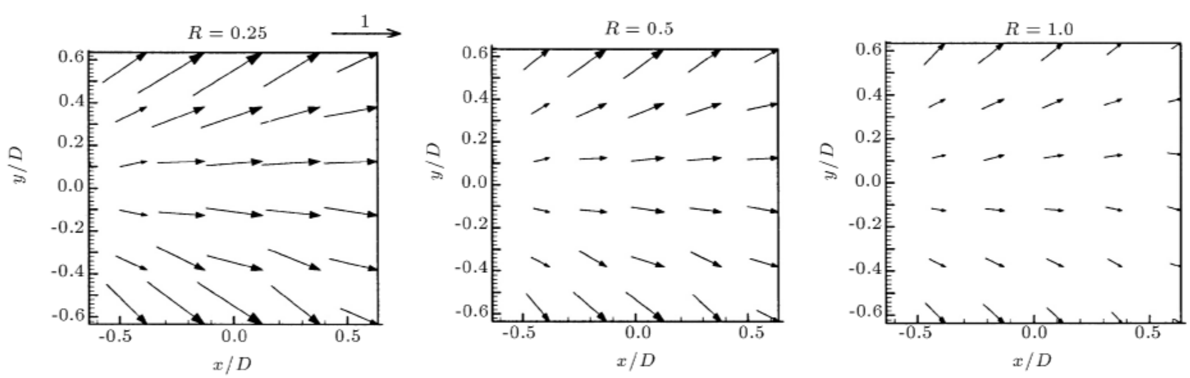

Figure 7. The velocity vectors in the plane of the jet exit.

contrast to high and low velocity ratio cases). Note, in all three cases, the trajectory of the jet is deflected into a streamwise direction, while the crossflow is altered as if it were blocked by a rigid obstacle. However, because of the jet entrainment effects and that of the motion of the jet (compared to a fixed body), the jet in the crossflow results are somewhat different (Figure 8). It is also shown from Figure 8 that the downstream region of the flow field consists of four known vortical structures: The horseshoe vortices, the jet shear layer, the wake structures and the Counter-Rotating Vortex Pair (CRVP). The horseshoe vortices from the upstream of the jet exit wrap around the exiting jet column. The jet shear layer consists of ring vortices in the jet boundary. The wake structures from downstream of the jet column persist and convect far downstream of the exit nozzle. The jet column then converts to the CRVP, the dominant vortical structure of the transverse jet (after the jet has turned in the crossflow direction).

In this study, two sources of vorticity in the jet in crossflow are identified: The crossflow and the jet exit

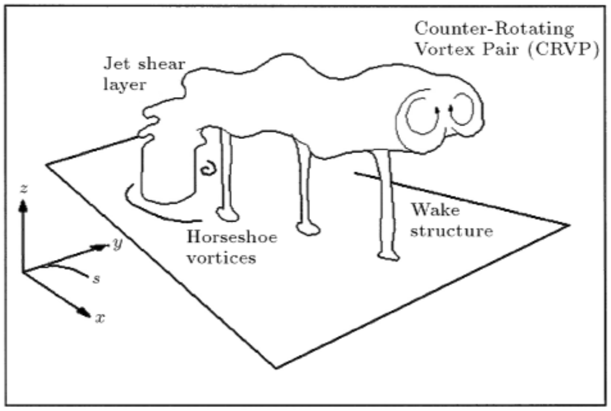

Figure 8a. The known vortical structures of the jet in crossflow [37].

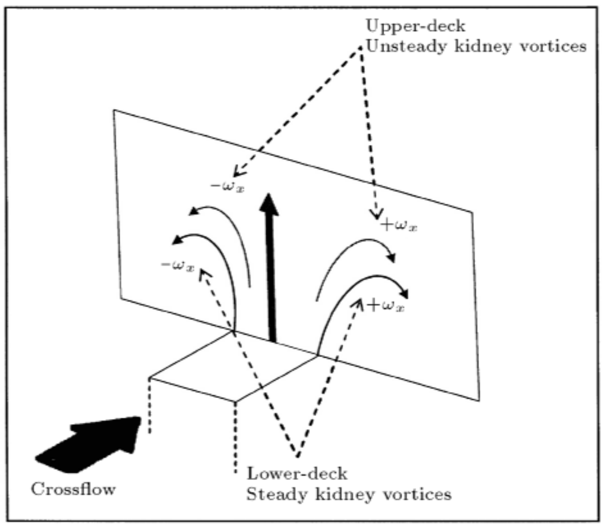

Figure 8b. Double-decked structure (kidney vortices) of the jet in crossflow [37].

boundary layer. Using smoke flow visualization, one can provide evidence that it is the crossflow boundary layer which provides the velocity of the wake structures. Also, the separation events of the crossflow boundary layer can be identified, which form vortices attaching to the lee side of the jet, turning up and becoming the wake structures. This turning-up mechanism is also seen in tornadoes. The kidney vortices are the downstream manifestation of the vorticity initially arising from the sidewall boundary layer of the hole passage. As illustrated in Figure 9, for the rectangular hole geometry, the sidewall of the hole generates vorticities aligned with the x-direction. This vorticity, after undergoing an intermediate growth stage, eventually appears in a far downstream plane oriented in the (y, z) plane as kidney-vortices $(\omega_x, \ \ \omega_x)$.

A more precise description, however, must also consider the vorticity which is not initially aligned with the x-direction. All vorticity originating within the jet

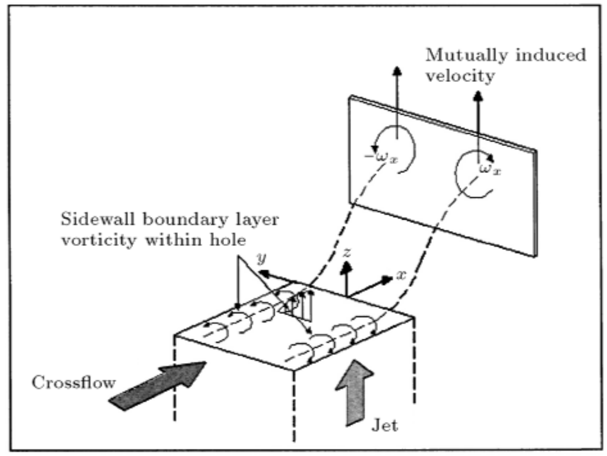

Figure 9. The kidney vortices due to hole sidewall vorticity [37].

is subjected to twisting and turning as the jet interacts with the crossflow. This means that the vorticity generated on the front and back walls of the hole, though not initially aligned with the x-direction, can be turned, such that additional x-components of the vorticity may appear in the (y, z) plane. The crossflow boundary layer can likewise be realigned due to the interaction with the jet. For all three-velocity ratios, a reverse flow region appears downstream of the jet exit, which assures the existence of a three-dimensional separation. The size of the reversed flow region for the large velocity ratio case ($R = 1.0$) is greater than that of the cases in which $R = 0.5$ and 0.25. Also, the reversed flow region for these two cases is localized much closer to the flat plate. This is due to the stronger deflection of the jet, which reduces the size of the low-pressure region.

The three-dimensional nature of the flow field is illustrated by the velocity fields and the streamlines of Figure 10. This figure shows the non-dimensional velocity vector fields and the streamlines at different spanwise planes ($x/D = 0$, 1, 3, 5 and 8) for $R = 0.5$ and 1.0, respectively. At $x/D = 0$, for all three velocity ratios, the vertical velocity component has a relatively large value. But, in the region where y/D is larger than 0.5, the transverse component of the velocity is dominant in the near wall region. The flow parallel to the wall is due to the injection of the jet, which results in pushing the crossflow fluid out in a transverse direction. From Figure 10, it is also observed that a CRVP starts to appear at $x/D = 1$ and its strength and its distance from the flat plate increase with velocity ratio. Also, the pressure drop in the wake region induces an inward motion, transporting the fluid from the crossflow towards the jet center-plane. Thus, at $x/D = 1$ plane, the somewhat irregular motion near the wall is due to the inward motion, which is balanced with the outward flow generated by the jet on either

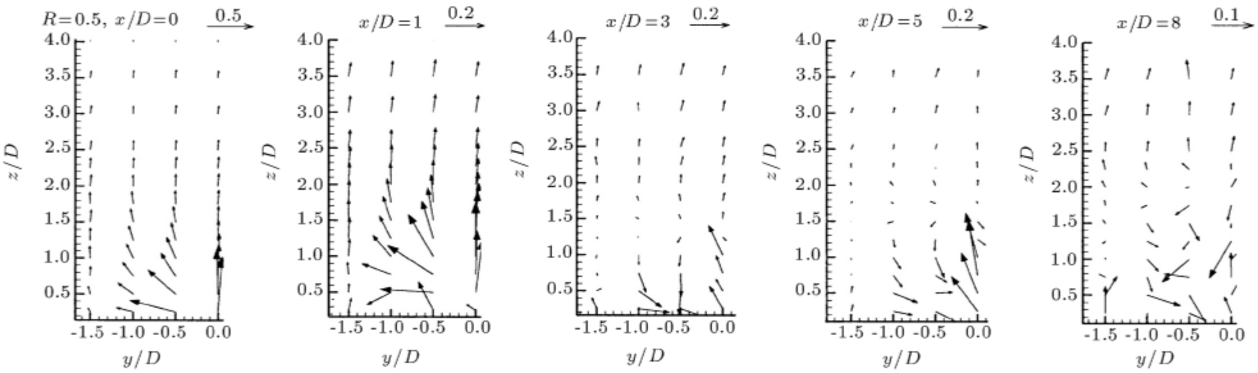

Figure 10a. The vectors normal to the main stream velocity in cross-tunnel planes for $R = 0.5$.

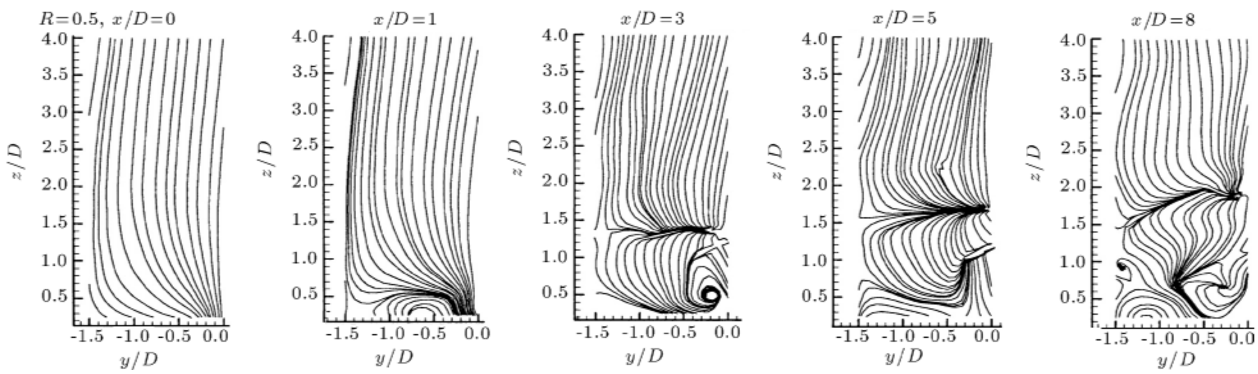

Figure 10b. The stream trace of flow field in cross-tunnel planes for $R = 0.5$.

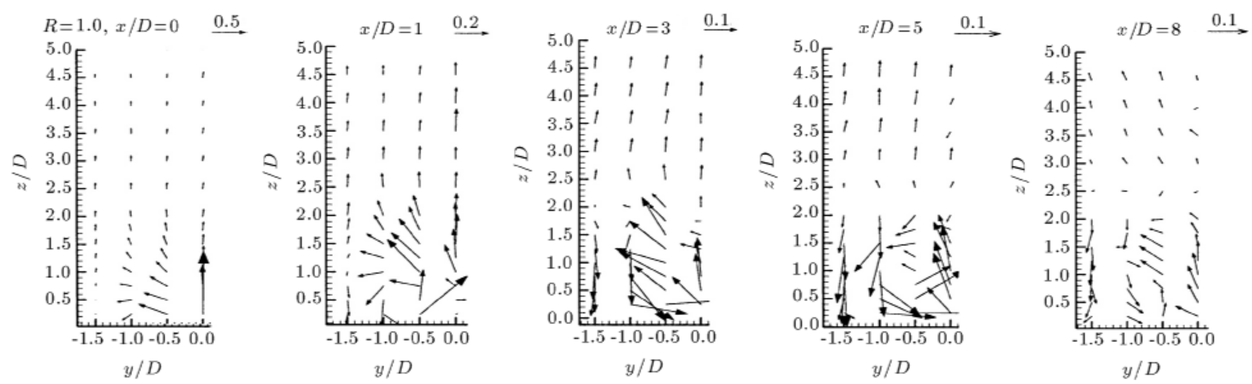

Figure 10c. The vectors normal to the main stream velocity in cross-tunnel planes for $R = l.0$.

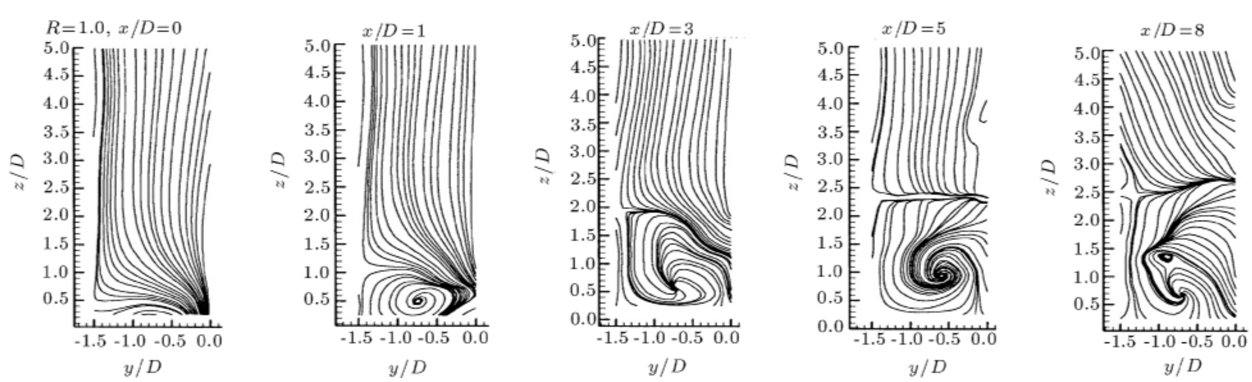

Figure 10d. The stream trace of flow field in cross-tunnel planes for $R = 1.0$.

side of the jet exit. Note that Figures 10a and 10c are comparable with Figure 3b for $R = 0.5$ and 1.0 at $x/D = 8$, which show close agreement.

Contours of the streamwise component of the velocity at different spanwise locations ($x/D = 0$, 1, 3, 5 and 8) for three different velocity ratios are shown in Figure 11. In the downstream location of the jet, a wake structure region appears, where the streamwise component of the velocity is relatively small. Also, note that the size of the wake increases, going from $x/D = 3$ to 8, while the wake structure grows with the velocity ratio. In addition, a shear layer exists above the wake region with a high streamwise velocity gradient. As one moves downstream, the jet effects decrease and the flow returns to its regular boundary layer type. For all three velocity ratios, the reversed flow region discussed earlier is apparent at $x/D = 1$ plane. Also, this region increases with increasing the velocity ratio. Note that Figures 11b and 11c are comparable with Figure 3a, for $R = 0.5$ and 1.0 at $x/D = 1$.

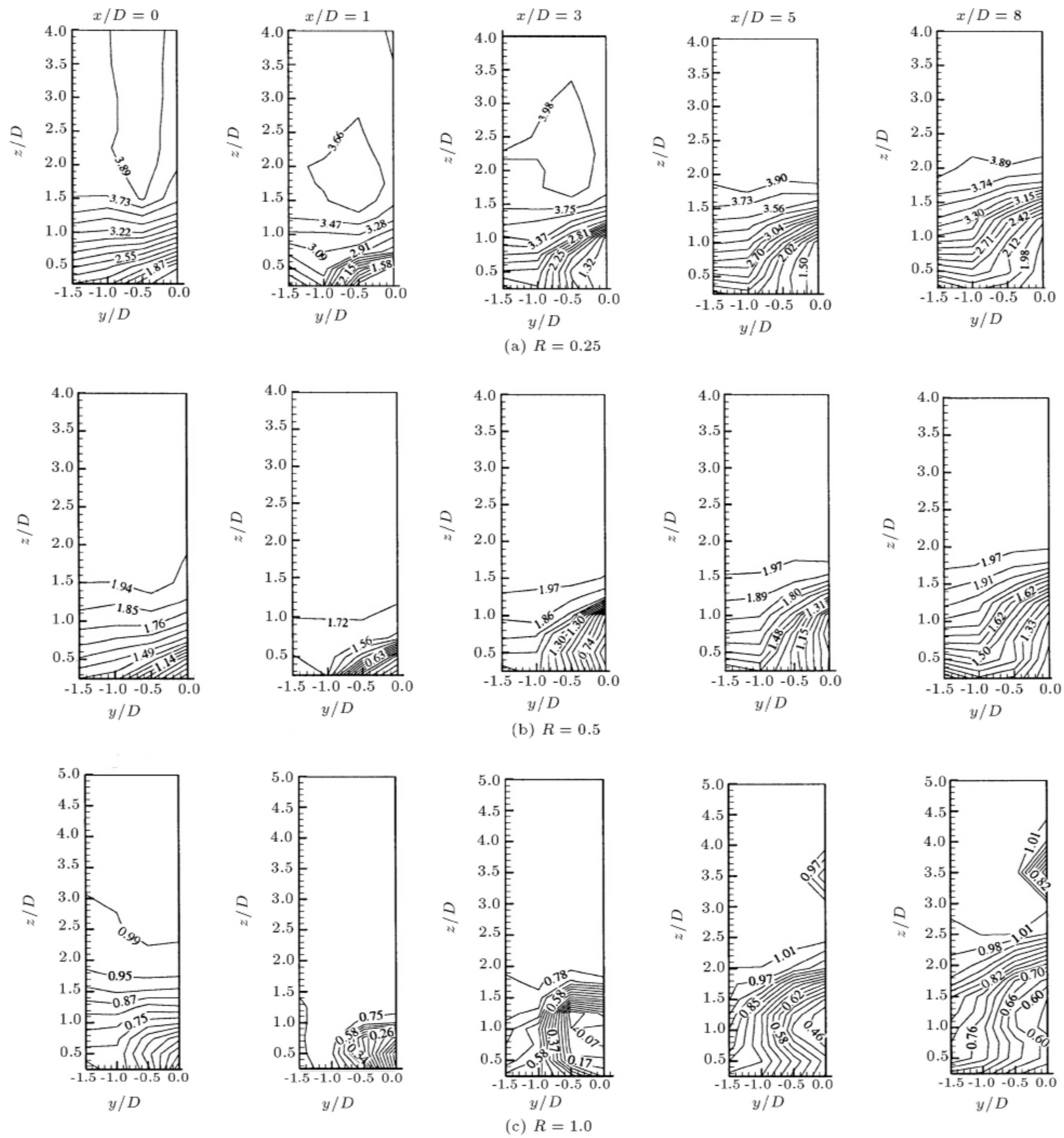

Figure 11. The distribution of the mean streamwise velocity at different spanwise planes for different velocity ratios.

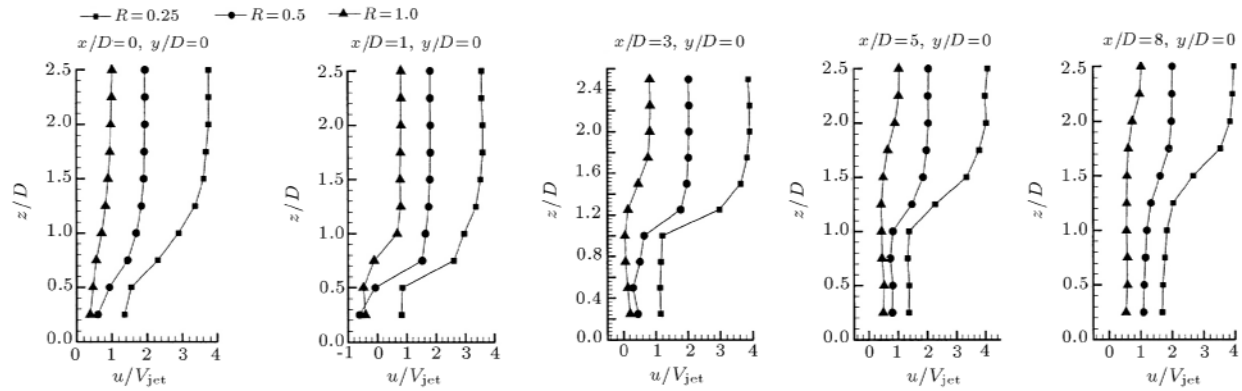

Figure 12. The streamwise velocity (u/V_{jet}) at jet center-plane ($y/D = 0$) for different velocity ratios.

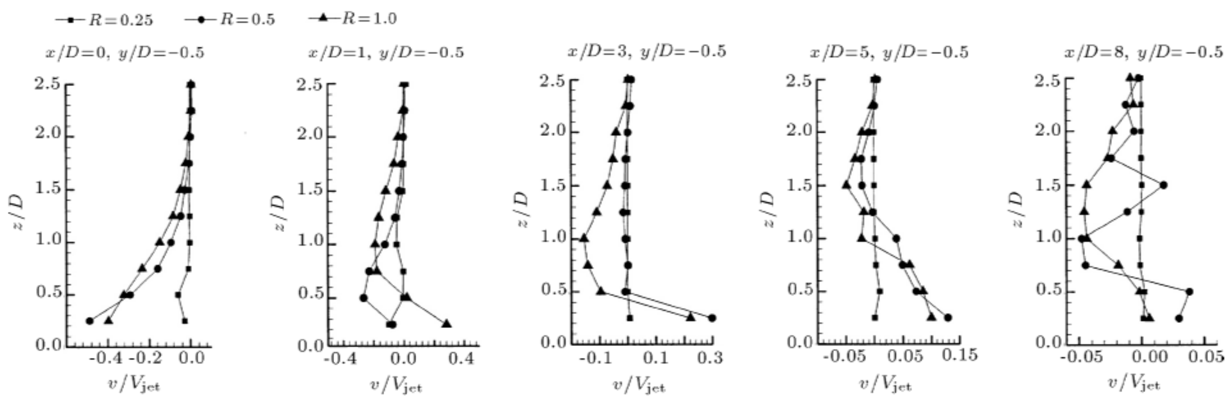

Figure 13. The cross-tunnel component of velocity (v/V_{jet}) at ($y/D =$ 0.5) for different velocity ratios.

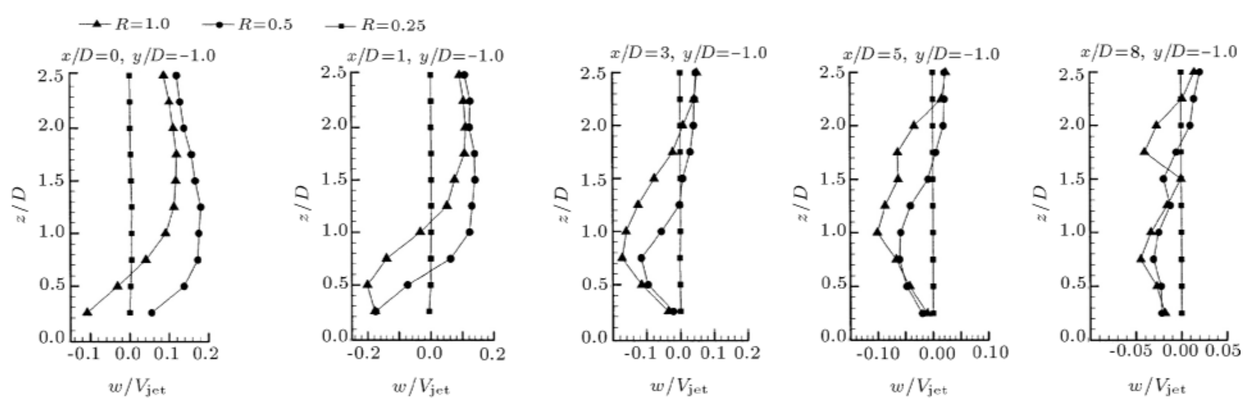

Figure 14. The vertical velocity (w/V_{jet}) at ($y/D =$ 1.0) for different velocity ratios.

Mean Velocity Profiles

The profiles of the streamwise velocity at the jet center-plane ($y/D = 0$) for different streamwise stations ($x/D = 0$, 1, 3, 5 and 8) and different velocity ratios ($R = 0.25$, 0.5 and 1.0) are shown in Figure 12. In all cases, the streamwise velocity in the jet wake is captured. This is particularly noticeable at $x/D = 3$. Note, Figure 12 is comparable with Figure 3c for $R = 0.5$ at stations $x/D = 0$, 1, 3, 5 and 8. Finally, Figure 13 shows the lateral component of the velocity at $y/D =$ 0.5, a plane which crosses the structures of CRVP, while Figure 14 shows the vertical velocity profile at $y/D =$ 1.0. Both of these figures show the down-flow, which exists on the outer edge of CRVP.

Reynolds Stress Distributions

Shear stresses are often left unmeasured and unreported due to the lack of suitable tools. However, in this study, a dual-sensor probe is used to measure the flow field characteristics. The profile of the shear stress

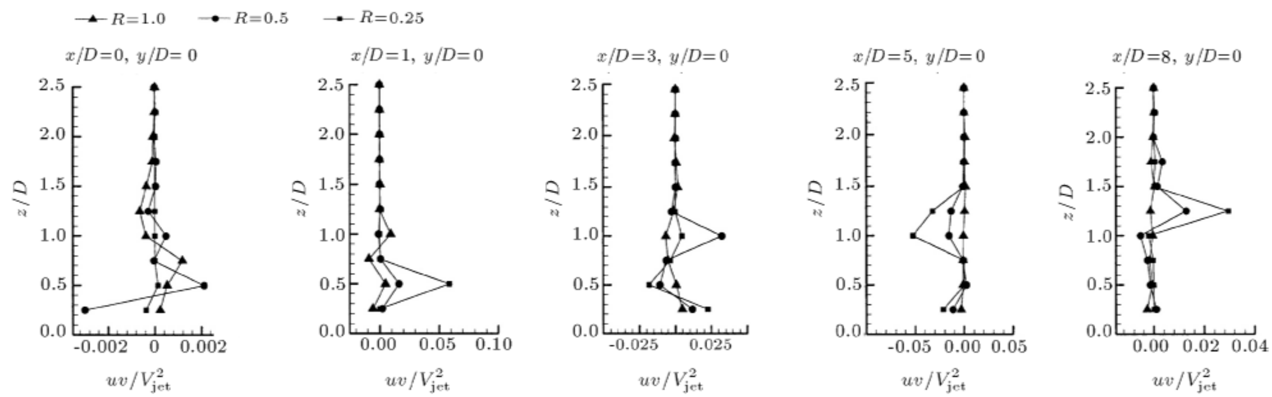

Figure 15. The shear stress $(\overline{uv}/V_{\text{jet}}^2)$ at $(y/D = 0)$ for different velocity ratios.

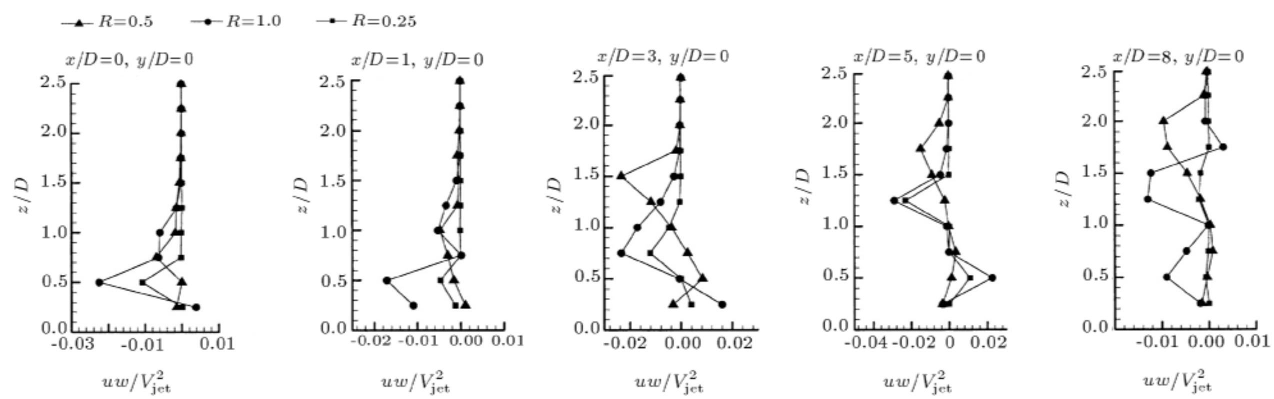

Figure 16. The shear stress $(\overline{uw}/V_{\text{jet}}^2)$ at $(y/D = 0)$ for different velocity ratios.

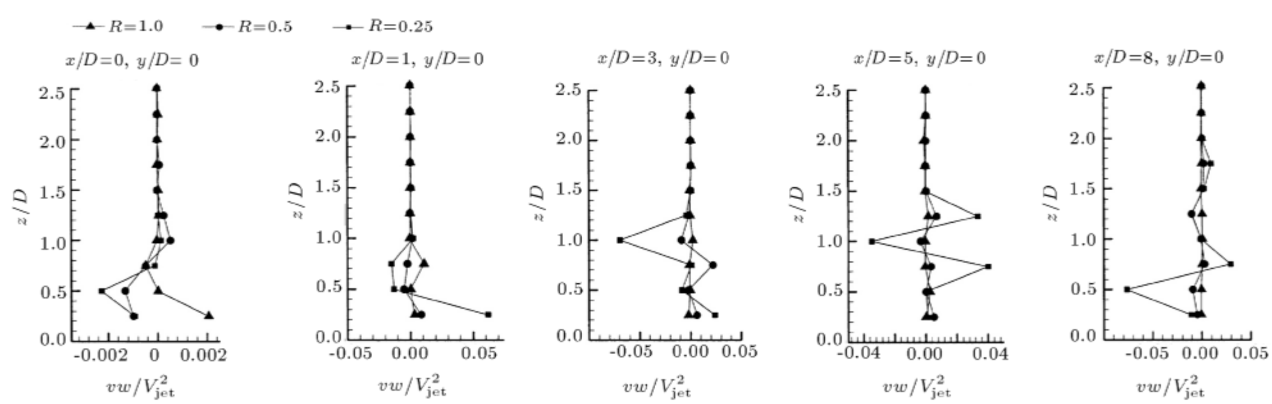

Figure 17. The shear stress $(\overline{vw}/V_{\text{jet}}^2)$ at $(y/D = 0)$ for different velocity ratios.

$(\overline{uv}/V_{\text{jet}}^2)$ in the jet center plane $(y/D = 0)$ at different streamwise locations for $R = 0.25$, 0.5 and 1.0 are shown in Figure 15. As expected, the shear stress is an indication of the lateral turbulent mixing. As a check for the experimental technique and for the symmetry of the jet injection, the values of $\overline{uv}/V_{\text{jet}}^2$ in the jet center-plane were measured, as well as in between different jets. This value should, by symmetry, drop to zero in the plane between jets.

Figure 16 shows the profile of the shear stress $(\overline{uw}/V_{\text{jet}}^2)$ in the jet center-plane at different streamwise locations for different velocity ratios. At locations $x/D = 3$, 5 and 8 downstream, shear stress is negative at the upper layer of the flow field for $R = 0.5$ and 1.0. This indicates the weak correlation between u' and w' at these regions. The profiles of the shear stress $(\overline{vw}/V_{\text{jet}}^2)$ in the jet center plane and $y/D = 0$ for all three velocity ratios are shown in Figure 17. As expected, in the near-field of the jets, the values of this shear stress for $R = 0.5$ and 1.0 are less that the other shear stresses at the same locations. In the case of $R = 0.25$, in particular, for $x/D \geq 1$, the value of the shear stress, due to the breakdown of large-scale organization, becomes negative and again becomes a positive peak far from the tunnel floor.

The contour plots showing the measured values of $\overline{vw}/V_{\text{jet}}^2$ are displayed in Figure 18. In the case of $R = 1.0$, in particular, for $x/D \geq 3$, a region of primarily negative shear stress rises in magnitude to a peak at approximately $y/D = 1$. The values of $\overline{vw}/V_{\text{jet}}^2$ are, generally, somewhat less that the other shear stresses at the same locations. This is partly due to the magnitude of the terms contributing to the production of this stress. The shear stress ($\overline{vw}$) acts to damp the secondary-vortex motion and it is the gradients $\partial v/\partial z$ and $\partial w/\partial y$ which generate this shear stress. These gradients, however, are weaker than those involved in the production of $\overline{uw}$ and $\overline{uv}$, which are $\partial u/\partial z$ and $\partial u/\partial y$, respectively. For this case, the resolution of the measurement field is not sufficiently refined, given that the structures of the jet lie much closer to the tunnel floor.

Figure 19 shows a series of contours of the shear stress $\overline{uw}/V_{\text{jet}}^2$ at different streamwise locations for velocity ratio $R = 1.0$. In the near jet region of $x/D \leq 1.0$, there seems to be little large-scale organization in the flow. A refined measurement grid is needed to reveal more information here. At downstream positions, one observes that $\overline{uw}/V_{\text{jet}}^2$ reaches a negative peak far from the tunnel floor. The negative contours define a shape not unlike a crescent above the jet, with the concave side facing downward. The negative value occurs here, since the crossflow far from the wall ($z/D \geq 1.5$) exhibits the characteristics of a boundary layer with positive $\partial u/\partial z$ and the turbulence level drops from a high value near $z/D = 2$ to its free stream value farther away. The positive peaks of $\overline{uw}/V_{\text{jet}}^2$ appear on the lower bound of the jet, but are weaker in magnitude. Based on Figure 11, $\partial u/\partial z$ is negative in this region. The weaker jet case shows the same trends as above: The crescent shape is evident and the regions of negative and positive $\overline{uw}$ are both observed.

The contours of $\overline{uv}/V_{\text{jet}}^2$ are shown in Figure 20 for various downstream locations and at $R = 1.0$. Some organization of this shear stress appears to exist by $x/D = 1$ and is clearly apparent at all subsequent locations downstream. The crescent shaped region in these contours is recognized clearly. However, it is located beside the jet, the plotted values are positive

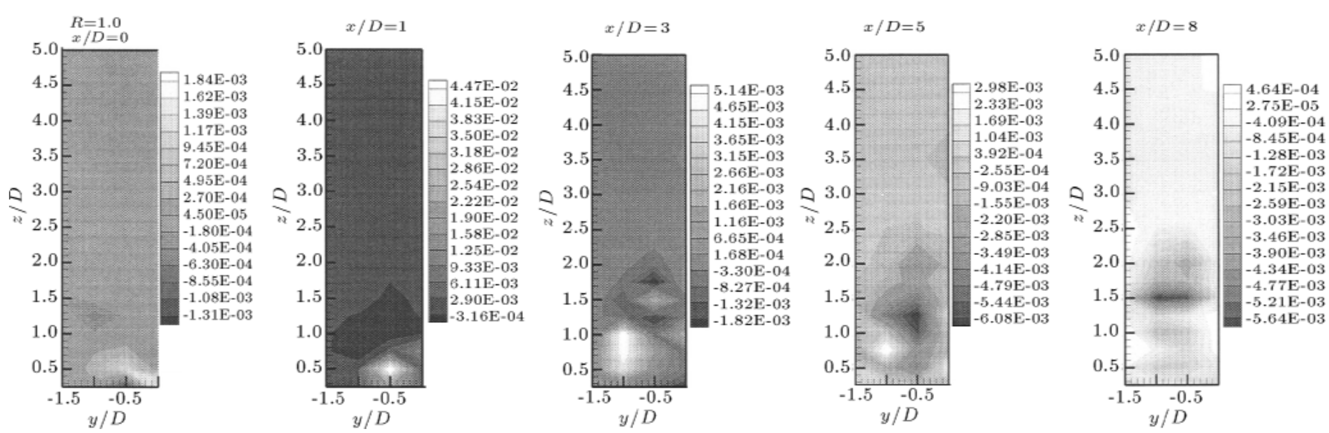

Figure 18. The shear stress ($\overline{vw}/V_{\text{jet}}^2$) in cross-tunnel planes.

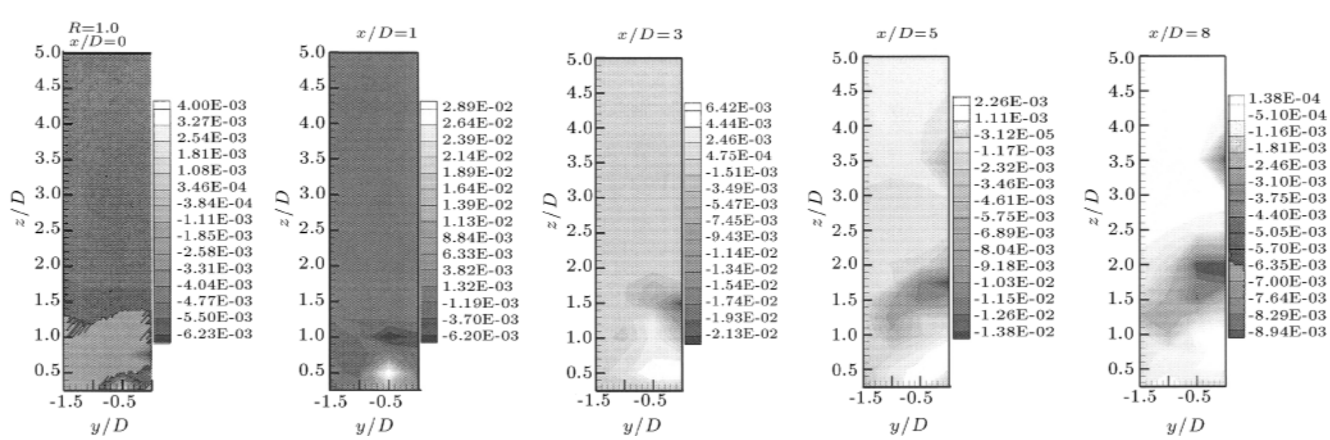

Figure 19. The shear stress ($\overline{uw}/V_{\text{jet}}^2$) in cross-tunnel planes.

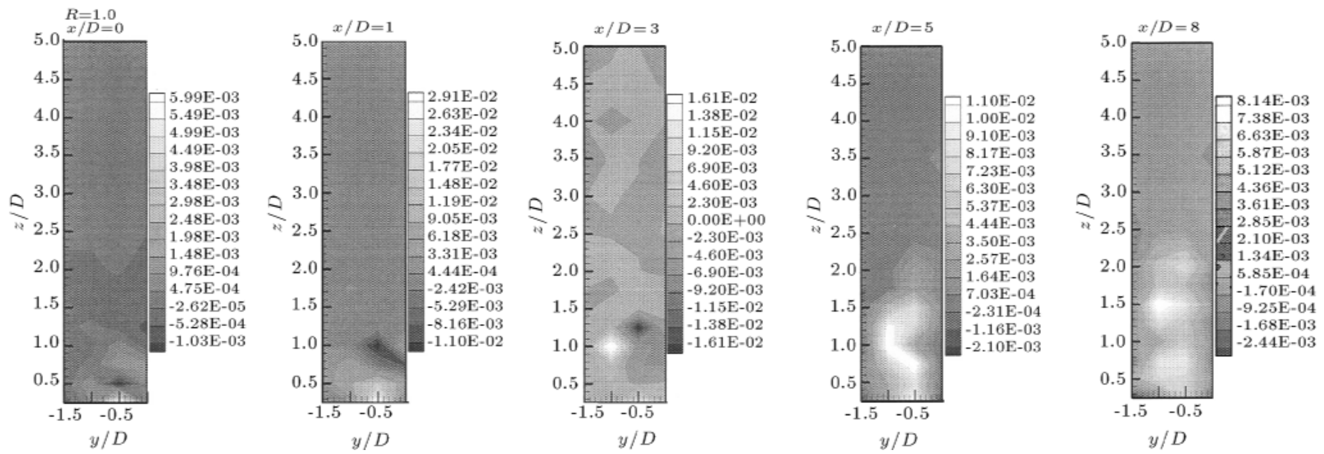

Figure 20. The shear stress ($\overline{uv}/V_{\text{jet}}^2$) in cross-tunnel planes.

and the concave side faces inward. One should expect to see a correlation between $\overline{uv}$ and the side bounds of the jet. The reason for this phenomenon exists in the wall of the jet channel, which expands in the axial direction. The shear layer circumscribes the jet and the spread of the turbulence is primarily normal to this shear layer. Therefore, the spread of the turbulence in a deflected jet should occur radially from the jet centerline with lateral spread occurring near the left and the right edges of the jet.

Turbulence Intensities

The profile of the turbulence kinetic energy ($\sqrt{k}/V_{\text{jet}}$) in the jet center-plane, at different streamwise locations for $R = 0.25$, 0.5 and 1.0, are shown in Figure 21. As shown in this figure, the turbulence kinetic energy is decreased by increasing the velocity ratio. For large x/D, the local minimum in the kinetic energy, which was measured in the wake region of the jet, shows a smooth distribution of turbulent kinetic energy, which rises to a peak away from the test-section floor. The location of this peak decreases and penetrates deeper with locations downstream.

The contours of the turbulence kinetic energy ($\sqrt{k}/V_{\text{jet}}$) are shown for several (y, z) planes for the velocity ratio $R = 1.0$ in Figure 22. The layout of the plots is similar to that of Figure 11c. Up to $x/D = 1$, in the case of $R = 1.0$, the turbulence levels near $z/D = 4.0$ are close to those measured in the free stream at $x/D =$ 5. Nevertheless, the influence of the jet is considerable, as one can see by following the penetration of the contour line ($\sqrt{k}/V_{\text{jet}} = 0.06$). This turbulence level is higher than that of the undisturbed free stream, but still far from that seen at the jet exit. This is used here to determine the extent of the jet penetration. At $x/D = 8$, the jet reaches a height of 2.7 D, which is deeper than the one that might be noted by examining the contours of u/V_{jet} or the vector plots in the (y, z) plane. A local minimum of turbulence kinetic energy occurs along the jet center-plane and approximately coincides with the minimums in u/V_{jet} in Figure 11.

As one would expect in a wake, the turbulence level decreases here with position downstream, dropping from 0.23 to 0.14 between $x/D = 3$ and $x/D = 8$. A peak in turbulence kinetic energy occurs at approximately $y/D =$ 1, beyond one diameter downstream. A comparison between the $\sqrt{k}/V_{\text{jet}}$ contours and the v w vector plots of Figure 10 shows

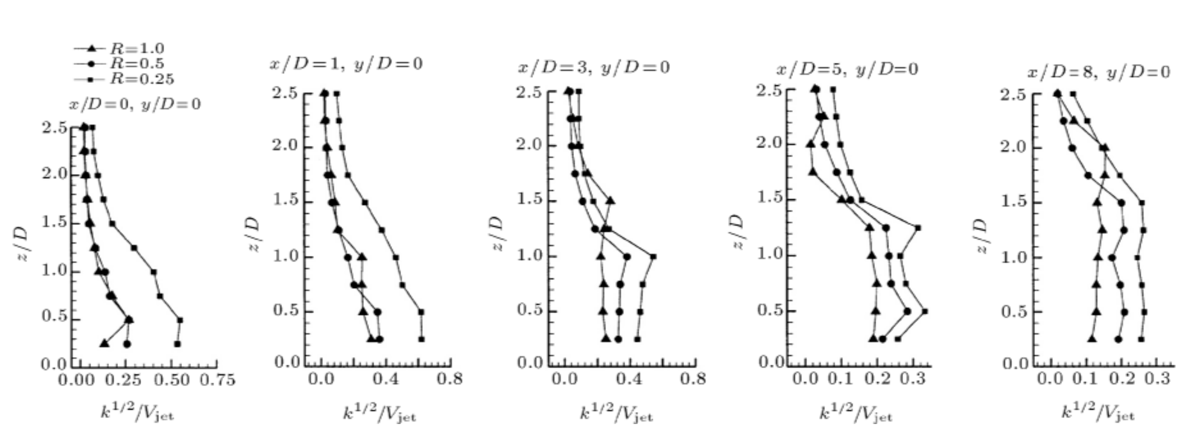

Figure 21. The turbulence kinetic energy ($\sqrt{k}/V_{\text{jet}}$) at ($y/D = 0$) for different velocity ratios.

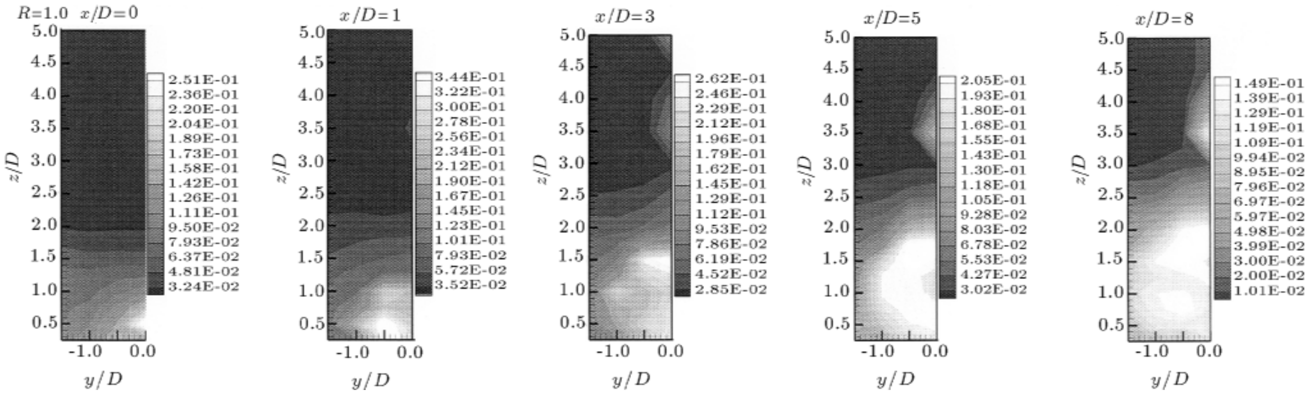

Figure 22. The turbulence kinetic energy ($\sqrt{k}/V_{\text{jet}}$) in cross-tunnel planes.

that the peak in $\sqrt{k}/V_{\text{jet}}$ occurs close to the edge of the vortex. The shear generated at the edge of the vortex promotes considerable mixing in this region. Also, any instability or unsteadiness in the position of the vortex would appear as an increase in turbulence kinetic energy at its edge, because of the shear layer moving through a fixed measurement point. Another local maximum first appears in the near wake region, occurring 0.5D above the tunnel floor at $x/D = 1$, where $\sqrt{k}/V_{\text{jet}}$ reaches 0.3. This region is one where the jet and the crossflow directly interact and may be characterized by instability and significant shear, thus, explaining the presence of high turbulence. This spot of maximum turbulence decays at downstream positions, but still persists and penetrates 1.75D by $x/D = 8$. Turbulence seems to spread out well in a lateral direction. From $x/D = 0$ to $x/D = 3$, strong gradients in $\sqrt{k}$, with respect to y, are evident, which suggest that turbulence has not yet spread to the plane of symmetry between jets. Downstream of this point, however, the levels of higher turbulence do reach $y/D = \quad 1.5$, which suggests that adjacent jets have merged. The distribution of the turbulence kinetic energy is similar for the $R = 0.5$ jet at $x/D = 8$. However, it differs for the case of $R = 0.25$. For this weak jet case, the turbulence levels in the plane of symmetry between jets are very close to those found upstream in the boundary layer. It would seem that the jets have not spread far beyond one diameter in a lateral direction and adjacent jets have, therefore, not merged.

Anisotropy

An examination of the turbulence kinetic energy provides valuable information about the turbulent nature of the flow. However, additional information is contained in the individual normal stress terms, which are not always the same. In this work, turbulence is shown to be non-isotropic with the magnitude of u' being approximately twice that of v'or w'. For the purpose of this discussion, only the case $R = 0.5$ is shown here. Figure 23 shows the contour plots of two normal stress ratios, defined as: $(v_{\text{rms}} \quad u_{\text{rms}})/u_{\text{rms}}$ and $(w_{\text{rms}} \quad u_{\text{rms}})/u_{\text{rms}}$, respectively, which are also called v' and w' ratios. A zero value of both ratios indicates that the flow is isotropic. Both plots correspond to the (y, z) plane at $x/D = 3$.

In the wake region of the jet, the v' ratio is about 0.29 and is representative of the flow at other downstream locations. This indicates that v' can exceed u' by 29% in the wake region, where the turbulence in the lateral direction is dominant. In the shear flow region, on the upper side of the jet, this ratio drops to -0.6. In this region, the velocity gradient $(\partial u/\partial z)$ is dominant and contributes to the production of u'. Here, v' is 60% lower than u'. The contours of w' ratio are mostly negative, but rise above zero in a small area in the wake region. A minimum value of -0.57 is found in an area in the shear flow region (on the upper side of the jet).

CONCLUSIONS

In the present experimental study, a three-dimensional flow field of normal jets in a crossflow was investigated.

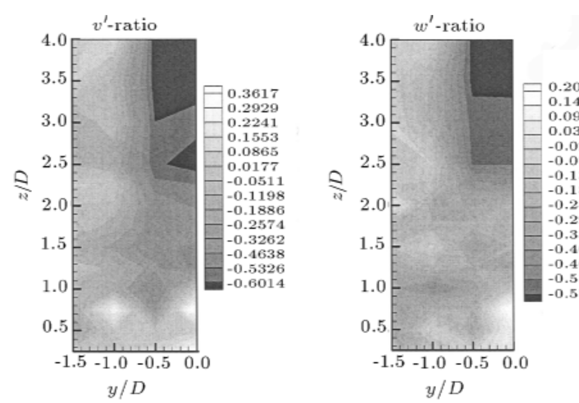

Figure 23. The normal stress ratio in cross-tunnel plane for $R = 0.5$ and $x/D = 3$.

The results of this experimental study were compared with the previous works for three different velocity ratios ($R = 0.25$, 0.5 and 1.0). Note that the same flow conditions used by Ajersch et al. [26] were utilized. However, in this study, the experimental setups in parts of the wind tunnel test section and the jets injection system are different. The flow field characteristics are captured by crossed hot-wire measurement techniques.

In comparison with Ajersch's results, the authors results show a similar unique physical behavior of jets in crossflows. As expected, the vertical velocity at the jet exit plane is non-uniform, particularly at low values of R. The counter-rotating vortex pair, the characteristics of most jets injected into crossflows, is observed in the present results for $R = 1.0$ and 0.5, but, is less distinct for $R = 0.25$, where the jet is too weak to penetrate through the turbulent boundary layer formed upstream of the injection. Note, also, that the adjacent jets appear to interact only for $R = 1.0$ and $R = 0.5$. However, when $R = 0.25$, the jet structures are eroded by the boundary layer before this interaction becomes possible. Note, also, that small back flow regions are observed just downstream of the jet in cases $R = 0.5$ and 1.0, while, for $R = 0.25$, this back flow region is weak and small.

On the other hand, in this study, turbulence is highly non-isotropic near the injection region, as expected. In a downstream region, the flow field can be divided into three regions: Wake, jet and free stream. In the wake region, there is a decrease in the streamwise component of the velocity. Also, downstream of the injection, the turbulence strongly differs from that of an undisturbed boundary layer. This study shows that hole geometry and its channel shape influence the very near-field character of the kidney vortices. The proximity of these counter-rotating vortices, relative to one another, affects both the lift-off of the jet and the entrainment of the crossflow fluid towards the plate surface. An unsteady, low frequency, asymmetric kidney vortex pair (which can be observed by flow visualization) may represent the instability arising from the streamline curvature.

ACKNOWLEDGMENT

This work was supported by research funds of Sharif University of Technology with Dr. Mohammad Kermanshah as technical monitor. The assistance of the Advanced Systems Research Center (ASRC) in manufacturing some parts of the experimental setup is greatly appreciated. Also, the authors would like to thank the staff of the Aerodynamics and Fluid Mechanics Laboratory at Sharif University of Technology for their cooperation.

NOMENCLATURE

D	jet diameter (jet width)
J	jet-to-crossflow momentum ratio
R	jet-to-crossflow velocity ratio
u, v, w	mean velocity components
U, V, W	total instantaneous velocity components
k	turbulent kinetic energy
S/D	jet spacing to jet diameter ratio
u', v', w'	fluctuating velocity components
$u_{rms}, v_{rms}, w_{rms}$	square root of normal stresses
$\overline{uv}, \overline{vw}, \overline{uw}$	shear stresses
ω_x	vorticity component in x direction
x, y, z	axes of the tunnel coordinates
$(\sim)$	denotes the magnitude of vector quantities
$()_{\mathbf{jet}}$	denotes jet
$()_{\mathbf{cf}}$	denotes crossflow

REFERENCES

1. Fric, T.F. and Roshko, A. "Structure in the near-field of the transverse jet", *7th Symposium of Turbulent Shear Flows*, pp 6.4.1-6.4.6 (1989).

2. Andreopoulos, J. "On the structure of jets in a crossflow", *Journal of Mechanical Engineering Science*, **138**, pp 93-127 (1985).

3. Sterland, P.R. and Hollingsworth, M.A. "Experiments on the flow in and around jets directed normal to a crossflow", *Journal of Mechanical Engineering Science*, **17**(3), pp 117-124 (1975).

4. Wieghardt, K. "Über das ausblasen von warmluft fur enteisen", *ARF Translation*, **F-TS- 919-RE**, Wright Field (1946).

5. Seban, R.A., Chan, H.W. and Scesa, S. "Heat transfer to a turbulent boundary layer downstream of an injection slot", *ASME Paper*, (58-A-104), pp 91-106 (1957).

6. Chin, J., Skirving, S., Hayes, L. and Silver, A. "Adiabatic wall temperature downstream of a single injection slot", *ASME Paper*, (58-A-104), pp 411-426 (1958).

7. Papell, S. and Trout, A.M. "Experimental investigation of air-film-cooling applied to an adiabatic wall by means of an axially discharging slot", *NASA*, **TN-D-9**, pp 312-319 (1953).

8. Hartnett, J.P., Birkebak, R.C. and Eckert, E.R.G. "Velocity distributions, temperature distributions, effectiveness and heat transfer for air injected through a tangential slot ratio into a boundary layer", *ASME Paper*, (65-A-105) (1961).

9. Goldstein, R.J., Eckert, E.R.G., Eriksen, V.L. and Ramsey, J.W. "Film cooling with injection through holes: Adiabatic wall temperatures downstream of a circular hole", *ASME Journal of Engnieering for Power*, **90**, pp 384-395 (1968).

10. Goldstein, R.J., Eckert, E.R.G., Eriksen, V.L. and Ramsey, J.W. "Film cooling following injection through inclined circular tubes", *Israel Journal of Technology*, **8**, pp 145-154 (1970).

11. Pedersen, D.R., Eckert, E.R.G. and Goldstein, R.J. "Film cooling with large density difference between the mainstream and the secondary fluid measured by the heat-mass transfer analogy", *ASME Journal of Heat Transfer*, **99**, pp 620-627 (1970).

12. Ito, S., Goldstein, R.J. and Eckert, E.R.G. "Film cooling of a gas turbine blade", *ASME Journal of Engineering for Power*, **100**, pp 476-481 (1978).

13. Katodani, K. and Goldstein, R.J. "On the nature of jets entering a turbulent flow", *ASME Journal of Engineering for Power*, **101**, pp 459-465 (1979).

14. Sugiyama, Y. and Usami, Y. "Experiments on the flow in and around jets directed normal to a crossflow", *Bulletin, JSME*, **22**, pp 1736-1795 (1979).

15. Sinha, A.K., Bogard, D.G. and Crawford, M.E. "Film cooling effectiveness downstream of a single row of holes with variable density ratio", *Trans. ASME, Journal of Turbomachinery*, **113**, pp 442-449 (1991).

16. Khan, Z.A., McGuirk, J.J. and Whitelaw, J.H. "A row of jets in crossflow", *Fluid Dynamics of Jets with Application to V/STOL*, **AGARD-CP-308**(10) (1982).

17. Afejuku, W.O., Hay, N. and Lampard, D. "Measured coolant distributions downstream of single and double rows of holes", *ASME Journal of Engineering for Power*, **105**, pp 172-177 (1983).

18. Isaac, K.M. and Jakubowski, A.K. "Experimental study of interaction of multiple jets in a crossflow", *AIAA Journal*, **23**(11), pp 1679-1683 (1985).

19. Forth, C.J.P., Loftus, P.J. and Jones, T.V. "The effect of density ratio on the film cooling of a flat plate", *AGARD Conference Proc. CP-390*, (10) (1985).

20. Pena, F.L. and Arts, T. "On the development of a film cooling layer", *Heat Transfer and Cooling in Gas Turbines*, **AGARD-CP-527**(36) (1992).

21. Foucault, E., Deniboire, P. and Bousgarbies, J.L. "Etude experimentale du transfert de chaleur pres d'une pario plane cauffee en presence d'injections multiples (ecoulement subsonique)", *Heat Transfer and Cooling in Gas Turbines*, **AGARD-CP-527**(4) (1992) .

22. Beeck, A., Fottner, L., Benz, E. and Witting, S. "The aerodynamic effect of coolant ejection in the leading edge region of a film-cooled turbine blade", *Heat Transfer and Cooling in Gas Turbines*, **AGARD-CP-527**,(35) (1992).

23. Benz, E., Witting, S., Beeck, A. and Fottner, L. "Analysis of cooling jets near the leading edge of turbine blades", *Computational and Experimental Assessment of Jets in Crossflow*, **AGARD-CP-534** (37) (1993).

24. Demuren, A.O. "Characteristics of three-dimensional turbulent jets in crossflow", *International Journal of Engineering Science*, **31**(6), pp 899-913 (1993).

25. Kim, S.W. and Benson, T.J. "Fluid flow of a row of jets in crossflow- a numerical study", *AIAA Journal*, **31**(5), pp 806-811 (1993).

26. Ajersch, P., Zhou, J.M., Ketler, S., Salcudean, M. and Gartshore, I.S. "Multiple jets in a crossflow: Detailed measurements and numerical simulations", *ASME Paper*, **95-GT-9**, pp 1-16 (1995).

27. Taeibi-Rahni, M. and Ebrahimi-Kebria, H.R. "Turbine blade film cooling numerical simulations", *CFD99-Proceedings of 7th Annual Conference of CFD*, Halifax Canada, pp 35-40 (1999).

28. Asif, H. and Acharya, S. "Predictions of a film coolant jet in crossflow with different turbulence models", *Journal of Turbomachinery, Transaction of the ASME*, **122**, pp 558-569 (2000).

29. Keimasi, M.R. and Taeibi-Rahni, M. "Numerical simulation of jets in a crossflow using different turbulence models", *AIAA J.*, **39**(12), pp 2268-2277 (2001).

30. Ramezani-Zadeh, M. and Taeibi-Rahni, M. "Large eddy simulation of multiple jets in a crossflow using Smagorinsky model", *Proceedings of the 5th Int. and the 9th Annual ISME Gilan Univ. Iran*, pp 293-299 (2001).

31. Cutler, A.D. and Bradshaw, P. "A crossed hot-wire technique for complex turbulent flow", *Experiments in Fluids*, Springer-Verlag, **12**, pp 17-22 (1991).

32. McQuaid, J. and Wright, W. "Turbulence measurements with hot-wire anemometry in non-homogeneous jets", *Int. J. Heat Mass Transfer*, **17**, pp 341-349 (1974).

33. Johnston, J.P. "Measurement in a three-dimensional turbulent boundary layer induced by a swept forward-facing step", *J. Fluid Mech.*, **42**, pp 823-844 (1970).

34. Bruun, H.H. "Hot-wire anemometry", Oxford University Press (1995).

35. Kline, S.J. and McClintock, F.A. "Describing uncertainties in single sample experiments", *Mechanical Engineering*, pp 3-8 (Jan. 1953).

36. Moffat, R.J. "Describing the uncertainties in experimental results", *Experimental Thermal and Fluid Science*, **1**(1), pp 3-17 (1988).

37. Aavani, K. "Experimental study of a crossflow on a flat plate for application to film-cooling phenomena", M.Sc. Thesis, Department of Aerospace Engineering, Sharif University of Technology, Tehran, Iran (2001).